Hindawi
Journal of Sensors
Volume 2019, Article ID 9570748, 14 pages
https://doi.org/10.1155/2019/9570748

Research Article

Time-Frequency Linearization of Reactive Cortical Responses for the Early Detection of Balance Losses

Giovanni Mezzina and Daniela De Venuto

Department of Electrical and Information Engineering, Politecnico di Bari, Bari 70125, Italy

Correspondence should be addressed to Giovanni Mezzina; giovanni.mezzina@poliba.it

Received 23 August 2019; Revised 10 November 2019; Accepted 7 December 2019; Published 31 December 2019

Guest Editor: Hassan Mostafa

Aiming at finding a fast and accurate preimpact fall detection (PIFD) strategy, this paper proposes a novel methodology that precociously discriminates the occurrence of unexpected loss of balance from the steady walking, by analyzing the subject's cortical signal modifications (at the scalp level) in the time-frequency domain. In this study, the subjects were asked to walk at their preferred speed on the treadmill platform programmed to provide unexpected bilateral slippages. The proposed PIFD method exploits synchronously recorded electromyographic (EMG: 2 channels from the same lower limb muscle bundle, bilaterally) and electro-encephalographic (EEG: 13 channels from motor, sensory-motor and parietal cortex areas) signals. To validate the method offline, also, the lower limb kinematics has been reconstructed via a motion capture system (23 reflective markers and 8 fixed cameras). During the PIFD system functioning, the EMG signals from the lateral gastrocnemii are first translated in a binary waveform and then used to trigger the EEG analysis. Once enabled via EMG (every gait cycle), the EEG computation branch extracts and linearizes the rate of variation in the EEG power spectrum density (PSD) for five bands of interests: θ (4–7 Hz), α (8–12 Hz), β I, β II, β III rhythms (13–15 Hz, 16–20 Hz, and 21–28 Hz). The slope of the linearized trend identifies, in this context, the cortical responsiveness parameter. Experimental results from six subjects revealed that the proposed system can distinguish the loss of balance with an overall accuracy of ~96% (average value between sensitivity and specificity). The discrimination process requests, on average, 370.6 ms. This value could be considered suitable for the implementation of countermeasures aimed at restoring the balance of the subject.

1. Introduction

The World Health Organization (WHO) statistics demonstrated that falls are a common occurrence and a serious health issue for the general population. In fact, in 2019, only in the United States, 29 million of falls have been recorded, resulting in 7 million of invalidating injuries. Moreover, it has been estimated that every 19 minutes an older adult die from a fall, while every 11 seconds an older adult is treated in the emergency room for the same reason. According to the Centers for Disease Control (CDC), falls are the leading cause of fatal injury among old adults and the most frequent reason for nonfatal trauma as well [1, 2]. These statistics support the clinical evidence according to which the natural aging process would alter the abilities to face the unexpected perturbations of the balance through the compensatory and anticipatory countermeasures [3, 4]. In this respect, the fall detection (FD) context arises with the main objective of creating systems, or devices, capable of detecting the fall events automatically in a short time and with good accuracy.

The first classification of FD strategies divides the algorithms into two macroareas: Postfall Mobility Detection (PFMD) and Preimpact Fall Detection (PIFD) algorithms.

The algorithms from the first macroarea (i.e., PFMD) detect the fall events when they already occurred. Typically, they assess the posthumous state of the subject mobility. The paradigm of these systems is as follows: (1) identify the fall, (2) evaluate the user mobility, and (3) call the assistance to avoid death due to "long-lie" phenomenon [5, 6] (the "long-lie" concerns the inability of elderly people to get up again after a fall event). The PFMD architectures present an intrinsic limitation: falls can only be detected as a result of

body-ground impacts; thus, it is not possible to prevent injuries directly caused by impacts. This limit can be overcome by using PIFD strategies [7, 8]. The PIFD architectures exploit techniques capable of recognizing the fall event before the body impacts in a disruptive manner with the ground [7].

Different from the PFMD techniques, the PIFD strategies require very short time to detect a fall event, trying to keep high accuracies in the fall recognition. Indeed, these strategies are designed and developed to be integrated into a closed-loop control system with on-demand fall protection devices or support for postural control. Although these systems are still under investigation and not already available on the market (if not for research purposes), the idea of merging PIFD strategies and protection countermeasures is considered a promising solution in the field of fall prevention [8]. Table 1 provides a detailed overview of PIFD strategies and solutions at the state of the art. The table shows, for each considered articles, the technology used to collect data for the fall detection implementation, the fall indicators, the classification method, the type of analyzed falls, and the performance in terms of sensitivity (Se), specificity (Sp), and average detection time (DT).

The devices used to detect fall early can be classified as context-aware devices or wearable devices. Among the works analyzed in Table 1, three studies [9–11] are based on context-aware technologies and coincide with those related to the recognition of falls from induced slipping. These studies use motion capture systems (MCS) as the main acquisition devices. MCS analyze kinematic determination by means of reflective markers placed on specific anatomical reference points of the human body. The trajectories of the markers are therefore traced by cameras mounted in fixed positions. The main pros of using MCS are that the fall indicators can be determined with extreme precision [7, 8, 12], while the main cons are the costs and the limited operating volume that can be framed by the cameras.

Table 1 presents some studies in which the detection of falls is made using a single type of wearable sensor [13–15]. The use of a single type of sensor has the advantage of significantly reducing the complexity and the computational request of the PIFD system [8]. Nevertheless, it has been demonstrated that, at present, the only acceleration signals do not allow to discern the phenomena of loss of equilibrium from activities like falls (e.g., running or jumping) [16]. Inertial measurement units (IMUs) solve the problem thanks to the simultaneous embedding of triaxial accelerometers and gyroscopes. Another interesting PIFD strategy is the one proposed in [17–22]. The authors propose a fully physiological signal-based cyber-physical system for fall detection. It consists of a wearable and wireless acquisition interface that exploits data from EEG and EMG.

The classification methods in Table 1 can be divided into the following: single and multiple threshold-based algorithms, machine learning-based approaches, or statistical models. Among the analyzed methods, the threshold algorithms are certainly the simplest in many aspects. Threshold-based algorithms are generally computationally efficient, suitable in real-time PIFD applications. Despite a fast detection, in most cases, these approaches provide accuracy below the 90%. To improve the PIFD strategy discrimination capability, realizing more efficient threshold-based systems, several solutions use ML methodologies [10, 14, 23]. Nevertheless, the ML algorithms request for a prolonged classifier training period. The authors in [17] analyze EEG and EMG signals by means of a logic-based matchmaking algorithm, which allows fast classification of the no voluntary movements. It is noteworthy that most of the solutions in Table 1 analyze simulated falls (SF), in which the subjects were asked to fall voluntarily or with specific postures. However, most real-life fall events occur due to unexpected perturbations and are characterized by an involuntary nature.

The performance of a PIFD strategy can be expressed in terms of accuracy and efficiency. The accuracy is defined by two parameters: sensitivity and specificity. Commonly, the sensitivity parameter is defined by the ratio between the number of correctly recognized fall events and the total number of evaluated falls. Similarly, the specificity can be defined as the ratio between the amount of successfully detected activities not identifiable as falls (e.g., walking steps) and the total number of these activities. The strategy efficiency is, instead, evaluated in terms of detection time, which is the time range from the perturbation initiation and the fall event recognition.

Ultimately, in terms of performance, Table 1 shows that the sensitivity of the proposed solutions ranges between 88% and 100% ($95.21 \pm 4.81\%$), while the specificity one between 88.5% and 100% ($94.59 \pm 5.14\%$). Data shows that the greatest problem of the proposed solutions (in term of accuracy) is related to the high number of false alarms, which reduce the specificity of the PIFD systems. It leads to overall system accuracies of $94.9 \pm 4.01\%$. Since the compensating actions related to the output of the PIFD strategy must be designed to avoid the falls, the detection times must be accurately estimated to demonstrate the temporal compliance of the system. In this respect, the authors in [24] set a detection time of 550 ms as the maximum intervention limit for the implementation of countermeasures aimed at restoring the balance of the subject. Data in Table 1 show that the detection time settles at around 559 ± 153.77 ms and, among the evaluated works, only the systems proposed in [10, 11, 15] provide detection times lower than the threshold of 550 ms, paving the way to their possible use in strategies for postural recovery. Other solutions are, instead, typically used to trigger total body or hip airbag-based protection systems, which can reduce the extent of the body-ground impact (that evolves in 700 ms-1000 ms).

In this context, the here proposed work is aimed at addressing the following challenges:

(i) To create a low compute-intensive algorithm that can analyze in time and frequency domain the reactive cortical dynamics (at the scalp-level) involved in balance adjustments when the steady walking is suddenly perturbed by slippages

(ii) To design a method to reach high values of accuracy (>95%), while maintaining detection time under the limit imposed by authors in [24]: 550 ms

Table 1: Overview PIFD strategies at the state of the art.

Ref.	Technology	Fall indicators	Class. Algorithm	Fall type	Performance
[13]	Trunk-positioned 3D ACC	Trunk vertical velocity (TVV)	Single Thr: TVV > 1.3 m/s	n. 3 SF: FwF, BwF, SdF	Se (%) = 100 Sp (%) = 98.27 DT (ms) = 577.00
[25]	Waist-positioned 3D GYR and ACC	Waist vertical velocity (WVV)	Single Thr: |WVV| > max WVV in nonfall activities	n. 4 SF: FwF, BwF, SdF, OrF	Se (%) = 100 Sp (%) = 100 DT (ms) = 675.15
[26]	9DoF IMU by Xsens Tech. positioned on chest	Acceleration and angular velocity of the chest segment	Multiple Thr: (1) acc.>7 m/s^2 (2) ang.velocity > 3°/s	n. 3 SF: FwF, BwF, SdF	Se (%) = 89.5 Sp (%) = 91.6 DT (ms) = 617.35
[14]	Trunk-positioned 3D ACC	Acceleration Time Series (ATS) of the chest	ML: (1) The extracted ATS trains a HMM (2) The HMM outcome is compared with a single Thr	n. 2 SF: FwF, SdF	Se (%) = 100 Sp (%) = 88.75 DT (ms) = 598.40
[23]	Waist-positioned 3D GYR and ACC	Acceleration and angular velocity of the waist segment	ML: (1) Mean and variance of the x, y, z axis acceleration and angular velocity (2) Classification by SVM	n. 4 SF: FwF, BwF, SdF, falling from sit IF: slip-induced fall	Se (%) = 93.5 Sp (%) = 85.6 DT (ms) = 775.20
[17]	EEG wireless headset+surface EMG	EEG Power Spectrum Density (PSD) level in BP, μ, β rhythms	Multiple Thr: (1) The EMG is used as a trigger for cortical analysis (2) The EEG PSD is evaluated in BP, μ, β bands (3) The levels are compared with history-based thresholds	n. 1 SF: BwF IF: loss of balance on weighbridge	Se (%) = 90 Sp (%) = 87 DT (ms) = 168 (from gastrocnemius contraction)
[9]	MCS: total body monitoring	Acceleration and vertical velocity of upper arms, trunk, tibia, and head	Multiple Thr+statistical model: threshold based on a ARIMA model based on data history	IF: slip-induced fall	Se (%) = 88.5 Sp (%) = 92.9 DT (ms) = 680.00
[10]	MCS: total body monitoring	Acceleration of all the monitored body segments	ML: (1) The accelerations are analyzed by ICA (2) A neural network is used to distinguish walk from perturbations	IF: slip-induced fall	Se (%) = 92.7 Sp (%) = 98 DT (ms) = 351.00
[11]	MCS+trunk-positioned IMU sensor	Sagittal angle and angular velocity of the trunk	Multiple Thr+statistical model: threshold based on a AR model based on data history	IF: slip-induced fall	Se (%) = 100 Sp (%) = 96.5 DT (ms) = 355.00
[15]	Hip encoder on active pelvis orthosis	Hip angle	Single Thr: increment of the error function between the current hip angles (from encoder) and the ones provided by a pool of adaptive oscillators	IF: slip-induced fall	Se (%) = 92.7 Sp (%) = 98 DT (ms) = 403.00

Technology acronyms—ACC: accelerometer; GYR: gyroscope; MCS: motion capture system; IMU: inertial measurement unit; DoF: degree of freedom. Class. algorithm acronyms—Thr: threshold; ML: machine learning; HMM: Hidden Markov Model; SVM: support vector machine; BP: Bereishaft potential (EEG); ARIMA: autoregressive integrated moving average; ICA: independent component analysis; AR: autoregression. Type of fall acronyms—SF: simulated fall; IF: involuntary fall (unexpected); FwF: forward fall; BwF: backward fall; SdF: lateral fall; OrF: fall from orthostatic position.

(iii) To realize a first-of-a-kind *fully* wearable sensor-based PIFD strategy in slippage recognition, which is typically entrusted to MCS

In this respect, the proposed study investigates changes in the cortical involvement when subjects were actively managing unexpected slippages delivered during steady walking. The proposed method synchronously records electrophysiological signals from 2 EMG electrodes placed bilaterally on the gastrocnemii and 13 EEGs along motor, sensory-motor, and parietal areas. The EMG signals from the lateral gastrocnemii are the first 1-bit digitized and then used as a trigger for the EEG analysis. During the cortical analysis, the system extracts the variation in the EEG power spectrum density for five bands of interest (i.e., θ (4–7 Hz), α (8–12 Hz), β I, β II, and β III rhythms) (13–15, 16-20, and 21-28 Hz) by using

the sliding window Fast Fourier Transform (FFT). The trend is then approximate by using a linear data fitting. The slope of the resulting linearized trend, m, identifies an approximate version of the clinical cortical responsiveness parameters.

Experimental results from six young and healthy subjects revealed a nonlateralized sharp increment of m just after the onset of the perturbation. Furthermore, the results show an interesting and concrete possibility of detecting the loss of balance induced by slips with good precision (96.02%) and with detection times shorter than the average of the state of the art (370.62 ± 60.85 ms).

The paper is organized as follows: Section 2 briefly defines the medical background, to facilitate the understanding of the detailed methodological bases of the algorithm. Section 3 discusses the experimental results providing a complete comparison with the state of the art, and Section 4 concludes the paper, presenting future perspectives.

2. Materials and Methods

2.1. Medical Background: Reactive Cortical Dynamics. Recent studies [27–36] have shown how the cerebral cortex regulates the excitability of subcortical postural centers to maintain the postural stability according to environmental demands [28]. Several studies on EEG signals [27–35] analyzed the cortical involvement in balance control. Typically, they focused on the study of event-related potentials (ERPs) elicited by mechanical perturbations of the subjects' balance. The proposed studies treated cortical reactions when the perturbations are provided to orthostatic posture [28, 29].

Few studies provided results about the reactive control spectral analysis [30–35]. They revealed important correlations among specific oscillatory rhythms, cognitive functions, and sensorimotor ones. Briefly, it has been proved [32, 33] that low-frequency cortical rhythms (<13 Hz) are related to perception and cognitive control. In a fall event context, the modulation of these oscillatory rhythms can be related to the visual field stabilization and active decoding of data coming from the vestibular system. Typically, these rhythms start oscillating in the first phase of the fall, involving the bands of interest: θ and α.

In a chronological order, the cortical involvement proceeds with the modulation of high-frequency cortical rhythms (>13 Hz). The latter are related to motor functions and in particular to the active concentration of the subject in muscle firing operations for the compensatory actions [34, 35]. According to the application-specific bands of interest, in this category, we consider the β bands (i.e., β I, β II, and β III). The power increase in the above-mentioned bands must be analyzed carefully. In fact, even during walking, cortical dynamics present significant impulses in the motor cortex side opposite to the leg muscles in the swing phase. Nevertheless, it is expected that the responsiveness of cortical activity observed during walking is, in any case, lower than the one expected during the postural recovery phase. Moreover, since the β bands are linked to the planning of sudden and precise changes, they are expected to not intervene in situations of unperturbed walking. Under this hypothesis, the power level in these bands could be considered one of the most discriminating parameters in the context of fall recognition.

2.2. Experimental Setup. The main goal of the study is to analyze the subjects' cortical reactive dynamics when during a steady walk (at their preferred speed) the balance is suddenly perturbed by unexpected bilateral slippages. In this respect, during the experimental trials, participants wore a 32-channel wireless EEG headset (g.Nautilus Research by g.Tec) and 2 wireless EMG surface electrodes (Cometa Wave Plus by Cometa Systems) as shown in Figure 1.

Table 2 provides information about the adopted acquisition equipment (i.e., EEG and EMG). For each device, the table reports the number of monitored nodes or channels, equipment features such as the size and weight, and the electrode characteristics and acquisition parameters: resolution and sampling frequency.

Thirteen EEG sites were monitored: F3, Fz, F4, C3, Cz, C4, Cp5, Cp1, Cp2, Cp6, P3, Pz, and P4, according to the international 10–20 system [37]. The O2 electrode was used for noise suppression, AFz as ground, and A2 (right earlobe) as the reference electrode. The EEG data were sampled at 500 Hz with 24-bit resolution [37].

Ten surface EMG channels were monitored from the following bilateral muscle groups: anterior tibialis, lateral gastrocnemius, vastus medialis, rectus femoris, and biceps femoris. The EMG signals were recorded with a sample rate of 2048 Hz and down sampled to 500 Hz (16-bit resolution) to match the EEG signal sampling frequency [22]. In this study, only EMG signals related to the lateral gastrocnemius were retained (two EMG surface electrodes).

Both EEG and EMG were transmitted via Bluetooth Low Energy (BLE) protocol to a dedicated gateway and collected by a Simulink model.

Figure 1, supported by data in Table 2, demonstrates the low encumbrance of the final architectures. The choice of fully wireless and light acquisition devices makes the preimpact fall detection architecture wearable. Despite this, since the use of gel-based or pregelled electrodes could not be considered comfortable, different solutions are still under investigation.

Figure 1 also shows a set of 23 reflective markers for the 3D kinematics reconstruction placed on the subjects' lower limbs and 8 cameras. Specifically, spherical markers ($d = 14$ mm) were mounted bilaterally on anterior superior iliac spines, sacrum, prominence of the greater trochanter external surface, lateral and medial epicondyle of the femurs, heads of fibula, lateral and medial malleolus, calcaneus, and first and fifth metatarsal heads. Additional markers were rigidly placed on wands over the midfemurs and midshaft of the tibia. It is important to stress that the MCS-oriented markers are only used for temporal coherence validation of the EEG/EMG signals and they are not part of the proposed architecture. In fact, kinematic records, electrophysiological signals, and the onset of the perturbation were synchronized offline on the same timeline for the system validation.

2.3. Experimental Protocol. During the experimental trials, subjects were asked to manage unexpected slippages while

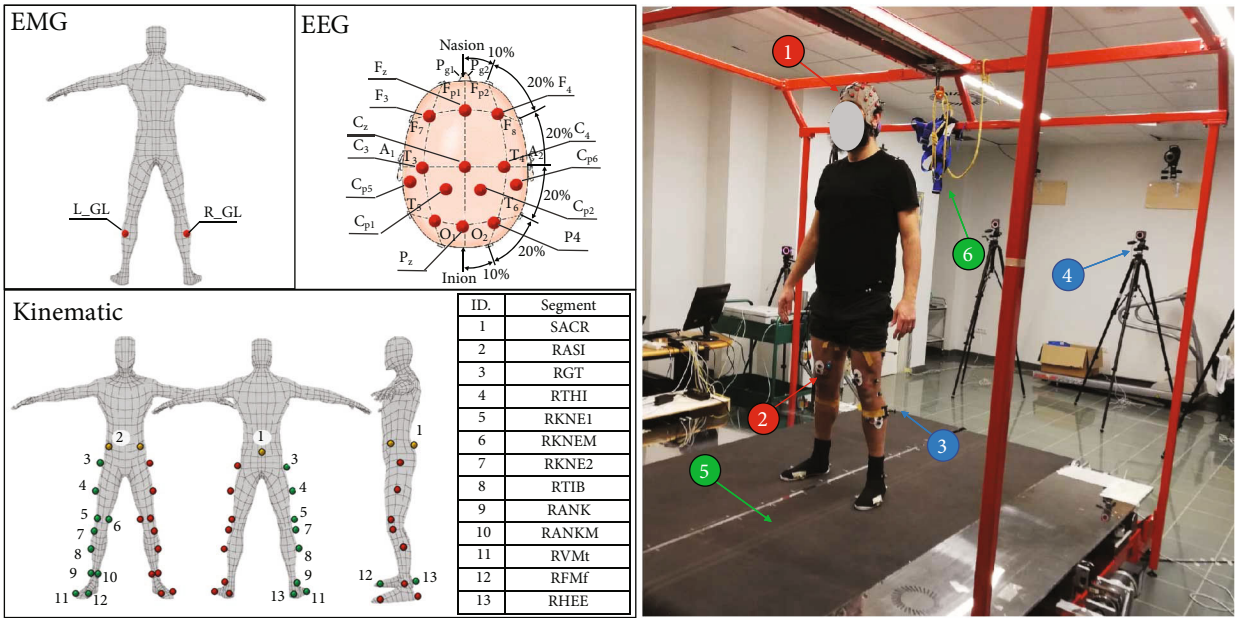

Figure 1: Experimental setup. The perturbation platform (SENLY) and a subject under test. On the figure, labels refer to the following: the wireless EEG headset (red: #1), the wireless surface EMG electrodes (red: #2), the set of markers (blue: #3), the motion analysis system camera (blue: #4), the perturbation platform SENLY (green: #5), and a safety harness (green: #6).

Table 2: EEG/EMG acquisition device features.

Sig.	Num.	Equipment features	Size (mm)	Electrode Type	Resolution	Sampling frequency
EEG	13 channels	EEG headset station: 70 × 55 × 30 mm Weight: 145 g Wireless 10 h continuous acquisition at 500 Hz	16 × 10 × 5	Active Gel based Sintered Ag/AgCl probe	24 bits	500 Hz
EMG	2 nodes	EMG single node: 33 × 23 × 19 mm Weight: 12 g Wireless 12 h continuous acquisition at 2048 Hz	18 × 12 × 5	Active Pregelled sintered Ag/AgCl holder ring	16 bits	2048 Hz ↓ 500 Hz

walking at their self-selected speed on a mechatronic platform named SENLY [38] (Figure 1—label #5). For safety reasons, the volunteers were secured by a harness attached to an overhead track.

SENLY is a platform designed to destabilize the balance control during motor tasks [38–40]. It consists of a split-belt treadmill, in which belts can be moved in the horizontal plane, both longitudinally and transversally. The platform is equipped with force sensors to identify the phases of the gait cycle during walking [40].

In the present study, the perturbations provided by SENLY consisted of sudden forward movements toward the anterior-posterior direction. Specifically, the selected belt was accelerated and decelerated up to the belt stop with a triangular speed profile (slope 8 m/s^2 for a total displacement of 0.15 m). The belt movement was triggered by detecting the heel strike of the foot appointed for the perturbation.

After the first acclimation phase (~5 min), the protocol consisted of a series of 10 consecutive trials in which the subject gait was perturbed by a slippage. The slippages were equally delivered alternating right foot-related belt and the left foot one.

2.4. The Preimpact Fall Detection Strategy. The work proposes an innovative solution in the field of PIFD strategies, whose primary goal is the real-time detection of a loss of balance through the synchronized analysis of physiological signals (i.e., EEG and EMG).

The block diagram in Figure 2 provides a general overview of the implemented architecture.

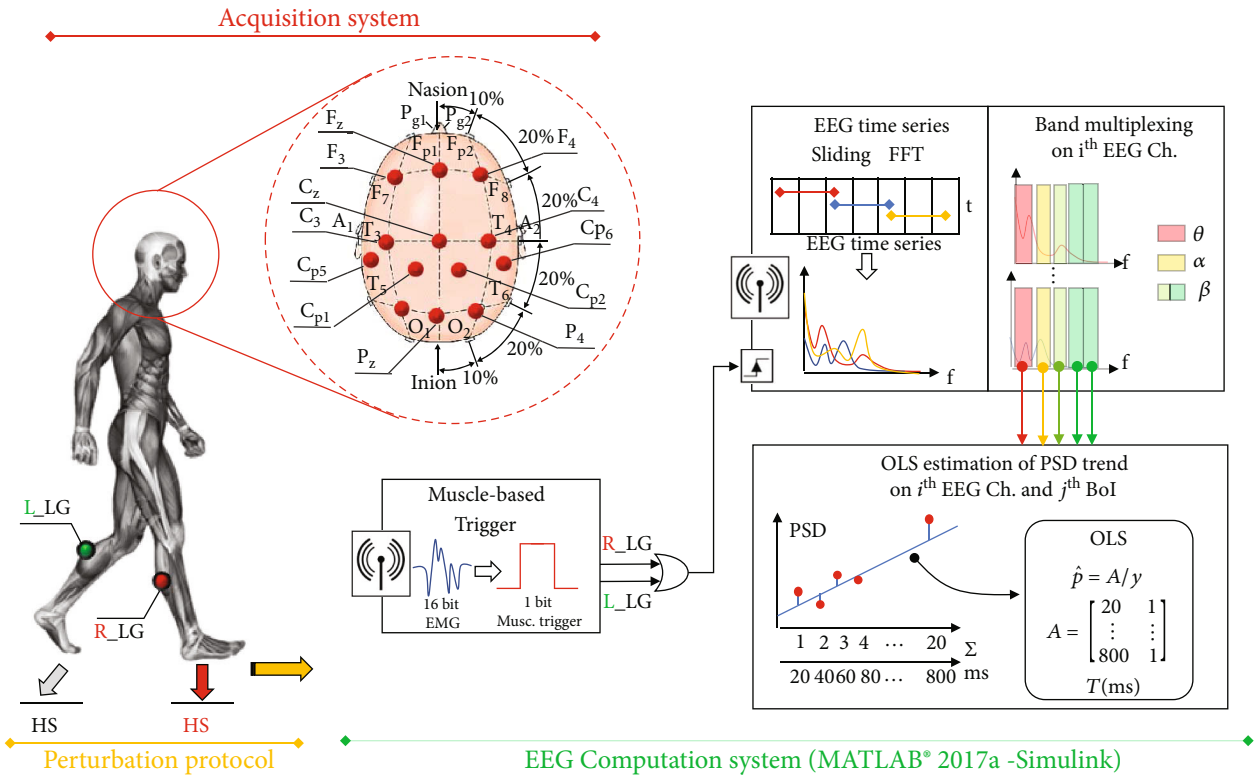

FIGURE 2: Overview of the proposed PIFD architecture. The block diagram recaps all the main procedure steps from signal acquisition to the PSD linear fitting extraction, which leads to final discrimination.

As shown in the figure, the system is composed of the three main parts: the acquisition system, the perturbation protocol, and the computing unit. The latter can be further divided in the EMG processing (i.e., Muscle-based Trigger) and the cortical analysis block that comprises the sliding window FFT, the band multiplexing process, and the ordinary least square (OLS) estimation of the power spectrum density trend.

From Figure 2, it is possible to notice how this architecture has been optimized and validated for the recognition of balance losses induced by SENLY as unexpected slippages (perturbation protocol—Figure 2).

As detailed in Section 2.2, the acquisition system in Figure 1 consists of an architecture that acquires and synchronizes EEG and EMG signals. Specifically, the system monitors 2 surface EMG surface electrodes placed on the lateral gastrocnemii (R(L)_LG—Figure 1) and thirteen EEG channels distributed between motor, sensorimotor, and parietal cortex. The acquired physiological signals (i.e., EEG and EMG) are then wirelessly transmitted to a common gateway that deals with synchronizing, in real time, the data coming from the two different acquisition systems.

In this work, the gateway consists of a receiving station connected, via USB, to a laptop on which a dedicated real-time Simulink-MATLAB®2017a model is running.

The Computing System working principle can be described as follows: The collected EMG signals are wirelessly sent to the first block (i.e., the Muscle-based Trigger) that translates the electrophysiological activity into binary signals. The trigger algorithm analyzes sample-by-sample the EMG, associating the value "1" to a contracted muscle, otherwise the value "0,"

This process of muscle activity digitization is entrusted to a moving average approach, which is able to adapt to changes in the subject's muscle tone [22]. These two binary waveforms are then used to independently trigger the cortical analysis. In this context, it was useful to identify a specific phase of the step cycle in which to activate the cortical analysis. This choice allows the system to exclude, from the total computation, the cortical activity that is not strictly linked to the specific movement, reducing the amount of data to be analyzed and possible occurrences of false alarms in the electroencephalographic profile. The trigger associated with this muscle is named Master Trigger (MT) in the following. We selected lateral gastrocnemius as MT because it uniquely identifies the double support phase of the gait cycle.

As previously stated, the rising edge of the MT enables the cortical analysis at every step (i.e., right and left gastrocnemius contraction independently). The EEG computing block quantifies the rate of variation in the power of brain signals, considering five interest bands by means of a sliding window FFT. Each window returns a power value in each evaluated band, building five vectors of measurements, named—for the reasons of generality—"y" in Figure 2. Then, the algorithm extracts, for each vector y a linear approximation of the PSD via ordinary least square (OLS) estimation. These models allow the system to extract, from the PSD measurement (y), two parameters ($\hat{p}$) via the matrix of base

function (A): the intercept and the slope of the resulting linearized PSD trend. The EEG responsiveness parameter practically consists in the slope. The EEG responsiveness parameters, extracted via linear models, contribute to the system calibration phase. In this stage, the system defines statistics-based models to identify the "standard" cortical behaviors.

During this phase, the implemented algorithm extracts a sequence of thresholds. The latter are then used to identify and classify all the statistically "nonstandard" behaviors (including the potential loss of balance) during the real-time operations. This classification phase is carried out by relating, among each other, the thresholds through a network of logical conditions. The network closes the processing, providing in the output the result of the binary classification: unperturbed step or potential loss of balance. If the output of the logical network is supplied in a time that is consistent with the fall dynamics, the system alert can be used to enable postural recovery strategies.

2.4.1. Data Preprocessing. The here-proposed system online treats the electrophysiological signals (i.e., EEG and EMG) following the following guidelines:

(1) EMG. Surface EMGs were on-line high-pass filtered with an 8th order Butterworth filter with cut-off frequency at 10 Hz to reject movement artifacts.

(2) EEG. According with the main studies in the field [28, 29, 36], the EEGs were progressively band-filtered between 1 Hz and 40 Hz by using an 8th order Butterworth filter before the transmission.

During every trial, an impedance check of all EEG electrodes was carried out in order to ensure a value lower than 40 kΩ.

A numeric notch filter (48-52 Hz) was implemented for both EEG and EMG signals.

(4) Special Precautions. EEG artifacts can be classified, in general, as physiological or non-physiological [41]. The former type includes eye movement (blinking, lateral and vertical movement), muscle contraction (tightening of the jaw, contraction of the neck muscle), and cardiac artifacts. The non-physiological artifacts include line noise, impedance shift, and interference from cable movement [41]. The acquisition of EEG signals during the gait increases the influence of these artifacts. Although there is no way to permanently delete all the above-mentioned artifacts, special precautions were taken during the recording sessions to limit their effects.

The use of active preamplified wet electrodes, with impedance check and fixing procedures of the electrode by PCB connection lines, guaranteed the attenuation of non-physiological artifacts. Moreover, in the experimental tests, the subjects were asked to fix their gaze on a frontal area at the eye level and to relax neck muscles during the experiment, avoiding, as far as possible, turning or swinging the head while walking.

To limit further confounding effects, the ambient lighting was kept constant, the ambient noise was reduced, and recording equipment and operators were kept out of the field of view.

The remaining artifacts will be rejected in the cortical analysis phase by embedding in the Simulink model an artifact rejection stage: the Riemannian Artifact Subspace Representation (rASR) method [42].

2.4.2. Muscle-Based Trigger Generation. As shown in Figure 2, the Muscle-based Trigger block is used to identify the onset of the contraction event for a specific muscle. For the particular application, in-depth knowledge of the EMG signal level is not as useful as knowing its binary approximation (e.g., ON/OFF). Although the ON/OFF condition conceptually and computationally simplifies the analysis of EMG signals, the algorithm of extraction of muscle triggers, presented in principle in Figure 3, must be able (i) to adapt to the characteristics of the muscle tone of the subject under test (intersubject variability) and (ii) to follow muscle tone changes during the trial.

In this respect, for this application, we refer to a method proposed in our previous works [22, 43] previously used in gait analysis applications. Briefly, it consisted of a dynamic threshold approach, in which each EMG signal (16-bit) was converted in a binary signal (named trigger). It assumes a logic value HIGH if the muscle is contracted, low otherwise (relaxed muscle). Figure 3 shows all the steps for the trigger generation.

The method, here, described in principle, compares the average of the signal power on a large time span of $M = 500$ ms (PM) and the signal power average on a shorter time span of $N = 250$ ms (i.e., the last 250 ms of the M register, PN). The process was refreshed sample-by-sample.

For the ith sample, PN was compared with the PM. If PN > PM, the trigger goes 1, otherwise 0.

2.4.3. The Cortical Analysis System. In this context, it has been experimented that the selected MTs (lateral gastrocnemii) typically react in 323.19 ± 52.38 ms to the slippages. From literature [36], we know that θ is the faster band (temporally) in intervening with a power variation (peak detectable at ~185 ms from perturbation onset) and therefore the most critical to be reconstructed, in the perspective of a fitting with a linear model enabled by MT.

In this respect, in this study, the system extracts an EEG time window that starts at 800 ms (i.e., 400 samples) before and ends at the MT contraction onset. As previously stated, the EEG subsets undergo the first stage of artifact rejection via rASR. The artifact-free EEG subset is then split in 20 overlapped (10-sample step) 200-sample long time windows.

On each evaluated time window, the system operates an FFT with a spectral resolution of 2.5 Hz ($f_{\text{sEEG}} = 500$ samples/s, $L_{\text{win}} = 200$ samples). The spectral behavior is then evaluated according to

$$Y = \left| \frac{\text{FFT}(s_w)}{L_{\text{win}}} \right| \rightarrow S = 2 \bullet Y\left(2 : \frac{L_{\text{win}}}{2}\right), \quad (1)$$

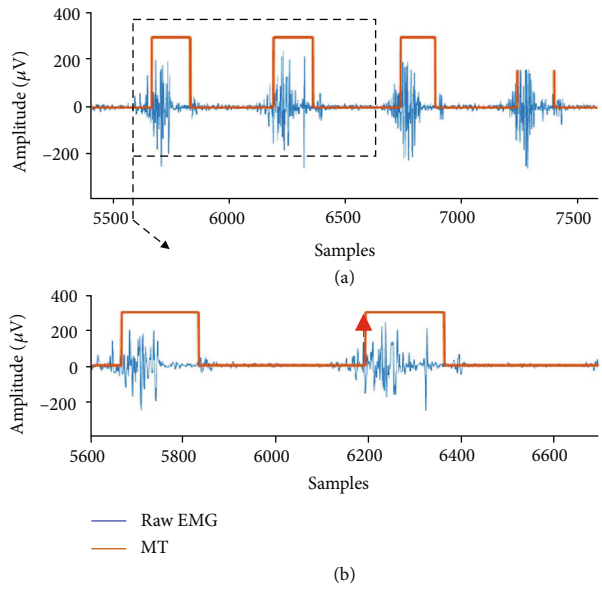

FIGURE 3: Overview of the muscle trigger extraction technique: (a) the Master Trigger (MT) is extracted from the raw EMG data; (b) detail of MT onset (red arrow).

where s_w is the 200-sample long sliding window to be evaluated and L_{win} is the number of samples that composes the analyzed data series. Once the spectral power $\mathbf{S} \in \mathbf{R}^{L_{\text{win}}/2}$ for each window has been extracted, the system starts with the band multiplexing phase according to Figure 2 [44, 45]. During the band multiplexing stage, the system extract the behaviors of θ (4–7 Hz), α (8–12 Hz) bands and the β I, β II, and β III (13–15, 16-20, and 21-40 Hz) rhythms taking into the account the spectral resolution. In this respect, for every analyzed window, the system extracts the vector $\mathbf{S}_{\text{BoI}} \in \mathbf{R}^{\text{nBoI}}$, with nBoI = 5, the number of bands involved in the multiplexing. This vector (i.e., $\mathbf{S}_{\text{BoI}}$) consists of the sum of all the spectral contributions falling within the range of the analyzed band, according to

$$\mathbf{S}_{\text{BoI}} = \begin{bmatrix} \theta \rightarrow \sum_{2}^{3} (S(i)) \Big|_{\text{dB}} \\ \alpha \rightarrow \sum_{3}^{5} (S(i)) \Big|_{\text{dB}} \\ \beta\,\text{I} \rightarrow \sum_{6}^{7} (S(i)) \Big|_{\text{dB}} \\ \beta\,\text{II} \rightarrow \sum_{8}^{10} (S(i)) \Big|_{\text{dB}} \\ \beta\,\text{III} \rightarrow \sum_{10}^{16} (S(i)) \Big|_{\text{dB}} \end{bmatrix} \in \mathbf{R}^{\text{nBoI},1}. \quad (2)$$

Ultimately, in correspondence of the MT contraction,

(1) The system extracts the vector $\mathbf{S}_{\text{BoI}}$ (equation (2)) for all the 20 sliding widows composing the EEG chunk to be analyzed

(2) All the vectors are embedded in a 2D matrix with a size of 20 × nBoI. Each column of this matrix recaps, in 20 points, the power spectrum measurements of a specific BoI in the 800 ms preceding the MT onset

(3) The computation is then extended to the monitored channel (nCh = 13), resulting in a 3D matrix $\mathbf{MS}_{\text{BoI}} \in \mathbf{R}^{20,\text{nBoI},\text{nCh}}$

Considering, for the sake of clarity, a single band of interest and a channel, the measurements related to the 20 windows are finally sent to a computation unit that deals with extracting linear models by means of least-square fitting (i.e., OLS estimation). In particular, this stage of cortical responsiveness computation is based on the simplified approximation that the brain response, described by 20 points, could be considered a straight line $x(t) = m \cdot t + q$.

Figure 4 shows a demonstrative and emphasized comparison (by referring to experimental basis), between a linear model extracted during walking (Figure 4(a)—blue) and a linear model from a reactive response to a perturbation (Figure 4(b)—red). Both the panels refer to channel F3 and the same band of interest (i.e., α). Data related to walking (Figure 4(a)) refer to MT onset #16 of the Sub. 4-Trial 2. The MT associated with the selected contraction was left gastrocnemius (ipsilateral to F3).

As the final step, system discards the information considered useless in this context, such as the estimated intercept, deriving a matrix that contains only the estimated slopes, $\hat{m}$. For each MT contraction, a 2D matrix is defined: $\mathbf{M} \in \mathbf{R}^{\text{nBoI},\text{nCh}}$, whose elements $m_{j,i} = \hat{m}|_{j^{\text{th}}_{\text{BoI}}, i^{\text{th}}_{\text{Ch}}}$ are the slope estimation of the above-described OLS-based model in the jth band of interest and ith channel. For example, in Figure 4, the degree of cortical responsiveness was extracted by the system in the case of unperturbed gait (MT #16) is $\hat{m}|_{\alpha,\text{F3}} = 0.0125$ dB/ms; similarly, in the case of perturbation (MT #41), this parameter is $\hat{m}|_{\alpha,\text{F3}} = 0.25$ dB/ms. Note that the x-axis reports the window number, and each window consists of a 20 ms step.

2.4.4. Logical Classifier. As stated in Section 2.4.3, the cortical analysis system extracts the cortical responsiveness matrix **M** for each evaluated contraction of the MT.

In the first calibration phase, the system collects several **M** matrices from unperturbed walking steps. Thus, it builds a statistic of the "standard" cortical behavior for the subjects under test.

More in detail, the system calibration requires the storage of the **M** matrices for a number, Nc, of unperturbed MT contractions. Once this data collection is over, a 3D matrix $\mathbf{MC} \in \mathbf{R}^{\text{nBoI},\text{nCh},\text{Nc}}$ is available for further computation. The general **MC** element, $\widehat{m_c}(j,k,i)$, represents the $\hat{m}$ value in the jth band of interest and kth channel extracted in correspondence of a generic ith MT contraction. By isolating the channel and band of interest data from the 3D cortical

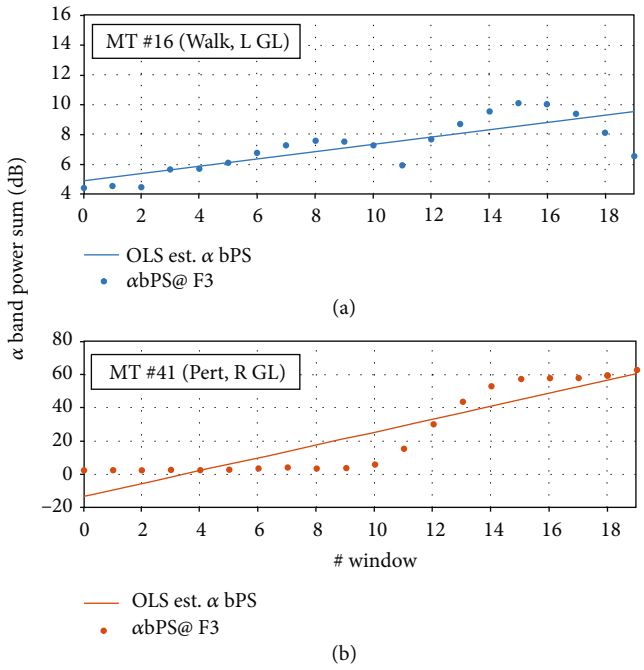

Figure 4: Comparison between OLS estimates of the sum of the powers in the α band in case of fluid walking (a) and perturbed one (b). Data refer the F3 channel.

response matrix (i.e., by selecting the kth channel and the jth band), it is possible to extract 65 vectors of size $\{1 \times Nc\}$. The 65 vectors extracted from the EEG branch of the architecture are then subjected to a *generalization* step, in which the system averages, on several channels, the values of $\hat{m}$ in a specific band. The resulting average constitutes groups of EEG channel called functional cortical groups. There are four functional cortical groups that roughly identify the monitored macroareas:

(i) Supplementary Motor Area. There are nBoI = 5 vectors, one per each band of interest, that include the $\hat{m}$ value averaged on the channels: {F3, Fz, F4}

(ii) Motor Area. There are nBoI = 5 vectors, one per each band of interest, that include the $\hat{m}$ value averaged on the channels: {C3, Cz, C4}

(iii) Sensory-Motor Area. There are nBoI = 5 vectors, one per each band of interest, that include the $\hat{m}$ value averaged on the channels: {Cp5, Cp1, Cp2, Cp6}

(iv) Parietal Area. There are nBoI = 5 vectors, one per each band of interest, that include the $\hat{m}$ value averaged on the channels: {P3, Pz, P4}

This step of generalization allows the system to obtain an immediate control on the general subject's cortical involvement status. Once the control structure has been made unambiguous by the generalization step, the calibration algorithm must statistically analyze only 20 vectors (5 BoI $*$ 4 functional groups). From these vectors, the system extracts the same number of thresholds based on percentile analysis. Specifically, all the thresholds coincide with the 95th percentiles of the analyzed vector. These thresholds are used to determine the initial state of the system (calibration). At the first contraction of the MT, the threshold will be updated by discarding the first value (the oldest in chronological order) and replacing it with the new one. In consideration of this last vector, the thresholds will be cyclically updated. Once the system is progressively recalibrated, the classifier analyzes the contribution of each functional group to the overall involvement.

The pseudocode in Pseudocode 1 summarizes and widely comments the routines of classification and the calibration considering a single band of interest.

More in details, according to row 1 the system compares the $\hat{m}$ values of each functional group (imX, with X acronym of the group) with the dedicated threshold (ThrX, with X acronym of the group). Then, if >50% of the evaluated groups are interested in a power increase in the cortical activity, a generalization flag (Gen_flag) is set to 1. The condition opens a second nested routine, the lateral_check one (row 5). This routine evaluates if the power increment interests only one side of the cortex (by means of the difference among $\hat{m}$ values from left side channels and right side ones). If the difference is below a certain tolerance, the lateralization flag (Lat_flag) is set to 1, indicating that the increase is widespread. If both the generalization and lateralization flags are set the system call the Alarm_on_BoI routine. It means that on the specific band of interest (e.g., α) the cortical activity is abnormal. If at least 3 bands of interest are interested in the widespread increase, the classification releases a global alarm, asking for an external intervention to restore the balance (potential fall detected).

3. Experimental Results

3.1. Participants. The fall detecting system has been validated on six young and healthy subjects, whose personal data and anthropometric measurements (mean ± std) are reported in Table 3.

No falls were reported during the trials. All participants were able to recover their balance.

Before starting the experimental sessions, all participants signed an informed consent. Research procedures were in accordance with the Declaration of Helsinki and was approved by the Local Ethical Committee (Prot. no. 0028266/2019).

3.2. PIFD Algorithm Performance. As introduced in Section 1, the metrics commonly used to quantify the performance of a PIFD strategy are the accuracy, in terms of sensitivity and specificity, and efficiency through the detection time [7, 8].

In the present study, the above-mentioned performance has been experimentally extracted by means of the protocol described in Section 2.3, asking the subject to carry out ten consecutive trials, with an intertrial time of 2 minutes (rest). The performance is computed on a final dataset of 60 perturbations (10 for each analyzed subject).

```
Routine: Logic Network Classification
Inputs:
MSMA; imSMA;   //MSMA: Vector of Nc m̂_c values from cortical group "Supplementary Motor Area"
                //imSMA: m̂ values from cortical group SMA @ ith MT contraction
MM1; imM1;     //MM1: Vector of Nc m̂_c values from cortical group "Motor Area"
                //imM1: m̂ values from cortical group M1 @ ith MT contraction
MS1; imS1;     //MSMA: Vector of Nc m̂_c values from cortical group "Sensory-motor area"
                //imSMA: m̂ values from cortical group S1 @ ith MT contraction
MPPC; imPPC;   //MM1: Vector of Nc m̂_c values from cortical group "Parietal area"
                //imM1: m̂ values from cortical group PPC @ ith MT contraction
Outputs:
Gen_Flag;   //Generalization Flag. It identifies a general cortical activity increment
Lat_Flag;   //Lateralization Flag. It identifies a NOT lateralized cortical involvement
Alarm_on_BoI ();   //The function is used to activate a warning flag on the specific evaluated BoI
        /* Body Program LogicNetwork_Classifier      */
1.  [Class] LogicNetwork_Classifier (imSMA, imM1, imS1, imPPC){
2.    CG_Sum = [imSMA>ThrSMA imM1>ThrM1 imS1>Thrs1 imPPC>ThrPPC]/4;
3.    if (CG_Sum>0.5) {
4.      Gen_Flag=1;
5.      Lat_flag=lateral_check ();
6.      if (Lat_flag == 1) {
7.        → call Alarm_on_BoI ();
8.      }
9.    }
10.   calibration (imSMA, imM1, imS1, imPPC); //refresh calibration values
11. }
      /*Example Calibration Step   */
12. [ThrSMA, ThrM1, ThrS1, ThrPPC] calibration(imSMA, imM1, imS1, imPPC) {
13. //In the first calibration section, the system embeds the extraction of the 95th
    percentile-based thresholds for every cortical group.
    ThrsMA = prctile (*MSMA, 95); ⋯; ThrPPC = prctile (*MPPC, 95);
14. //In the second one, the vector is automatically updated with the new "im" value, preparing the system for the next contraction.
15. *MSMA(0) = [];   *MSMA=[*MSMA imSMA]; ⋯;   *MPPC(0)=[];   *MPPC=[*MPPC imPPC]
16. }
```

Pseudocode 1: Pseudocode of logic network classifier routine and system calibration.

Table 3: Data and anthropometric measurements of the analyzed subjects.

Features	Value
Age	28.3 ± 5.1 years
Height	1.72 ± 0.06 m
Weight	65.2 ± 9.4 kg
Gender distribution	83% M, 17% F
Walking speed	1.11 ± 0.07 m/s

3.2.1. PIFD Algorithm Performance: Accuracy. Table 4 summarizes the system performance in terms of the following: muscular response side, number of active cortical groups, number of false alarms, and, finally, sensitivity and specificity. The "response side" column identifies the lateral gastrocnemius which first intervenes to try avoiding the fall. The experimental results show that in the presence of a balanced perturbation delivery (50% on the life side, 50% on the right one), subjects react the 57.22% of the cases by contracting the left gastrocnemius. This value does not consider the missing data (MD) due to misclassifications. The report shows how three subjects (Subs 1, 5, and 6) potentially react according to the medical literature [12, 36] by contracting the gastrocnemius of the unperturbed leg to restore balance. In the remaining cases, an anomalous stiffness on the right limb was recorded.

The "active cortical groups" column identifies the number of functional cortical groups usually above the thresholds, averaged on the 5 bands of interest. In this respect, Table 4 shows how, on average, a "nonstandard" neural behavior is detected on the 3.24 ± 0.73 cortical groups (mean and standard deviation on 5 bands of interest) in the presence of perturbation (F—Table 4). Similarly, the cortical groups actively involved in the steady walking (W—Table 4) are, on average, 1.66 ± 0.37. The results support the theoretical hypothesis behind the logical network classification: a widespread (not lateralized) and general cortical activity increment could identify a possible loss of balance.

Table 4 also shows how the proposed system can reach an overall sensitivity of Se (%) = 93.33 ± 5.16% and a specificity of Sp (%) = 98.91 ± 0.44%, fully competitive with the state of art. A quantitative comparison with the above detailed state-of-the-art solutions is shown in Figure 5.

Table 4: PIFD performance report: accuracy.

Sub.	Response side	Active cortical groups	False alarms	Se (%)	Sp (%)
1	R: 50% L: 40% 10% MD*[1]	F: 3.22 ± 0.83 W: 1.70 ± 0.82	3	90.00 (9/10)	99.22 (386/389)
2	R: 40% L: 60%	F: 3.10 ± 0.73 W: 1.50 ± 1.17	5	100.00 (10/10)	98.32 (292/297)
3	R: 30% L: 60% 10% MD*[1]	F: 3.10 ± 0.73 W: 1.80 ± 0.83	4	90.00 (9/10)	98.71 (308/312)
4	R: 20% L: 70% 10% MD*[1]	F: 3.20 ± 0.78 W: 2.30 ± 1.15	5	90.00 (9/10)	98.55 (339/344)
5	R: 50% L: 40% 10% MD*[1]	F: 3.20 ± 0.78 W: 1.20 ± 1.22	2	90.00 (9/10)	99.46 (370/372)
6	R: 50% L: 50%	F: 3.10 ± 0.73 W: 1.50 ± 0.97	3	100.00 (10/10)	99.20 (374/377)
Average 1 to 6	R: 42.77% L: 57.22% ± 13.40%	F: 3.14 ± 0.06 W: 1.67 ± 0.37	3.67 ± 1.21	93.33 ± 5.16	98.91 ± 0.44

*[1]MD: missing data due to misclassification; F: fall; W: steady walking.

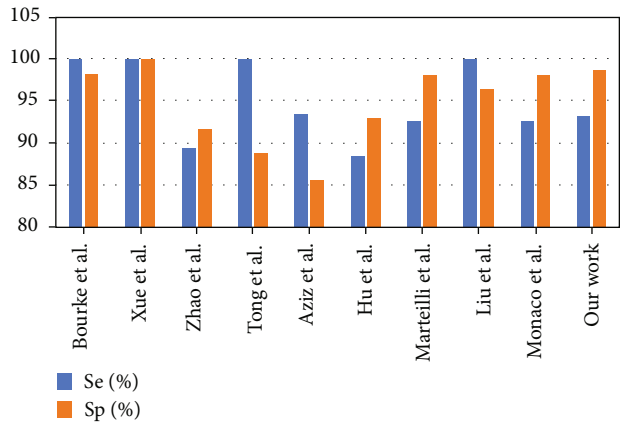

Figure 5: State-of-the-art comparison about the accuracy parameter of PIFD strategy.

3.2.2. PIFD Algorithm Performance: Efficiency. The efficiency of a PIFD strategy is typically evaluated in terms of time interval to reliably detect a loss of balance. This parameter can be derived as the time interval between the perturbation onset and the loss of balance status recognition. In this context, the proposed system has been validated by a motion capture system (MCS) to obtain, with proper precision, the perturbation onset provided by the SENLY platform in anterior-posterior direction on the selected limb.

The detection time, extracted during the experimental tests, is summarized in Table 5. They are computed considering the perturbation onset instant as the voltage step supplied to SENLY via Vicon Nexus software programming (MCS). The time resolution of this rising edge is ≤10 ms, but conservatively, we considered it in the detection time.

Table 5: PIFD performance report: efficiency.

Sub. ID	Speed (m/s)	Operating time (ms)	Detection time (ms)
1	1.05	21.753 ± 0.015	369.83 ± 97.49
2	1.10	21.744 ± 0.012	436.72 ± 86.66
3	1.00	21.739 ± 0.008	299.76 ± 107.99
4	1.15	21.751 ± 0.014	355.85 ± 151.38
5	1.18	21.750 ± 0.012	446.72 ± 112.89
6	1.17	21.654 ± 0.011	314.82 ± 105.34
Average 1 to 6	1.11 ± 0.07	21.732 ± 0.035	370.62 ± 60.85

In Table 5, the "operating time" column shows the computation time associated with the complete Computing System (Figure 2) working flow, which comprises (i) muscle trigger activation, (ii) sliding window FFT, (iii) band multiplexing, (iv) generalization and lateralization step, (v) logic network based classification, and (vi) recalibration of thresholds.

More generally, the report in Table 5 shows that, on six analyzed subjects, the implemented system requires, on average, 370.62 ± 60.85 ms to detect the induced fall. More in detail, the only Computing System (Figure 2) demands, on average, for 21.732 ± 0.035 ms to conclude the above-

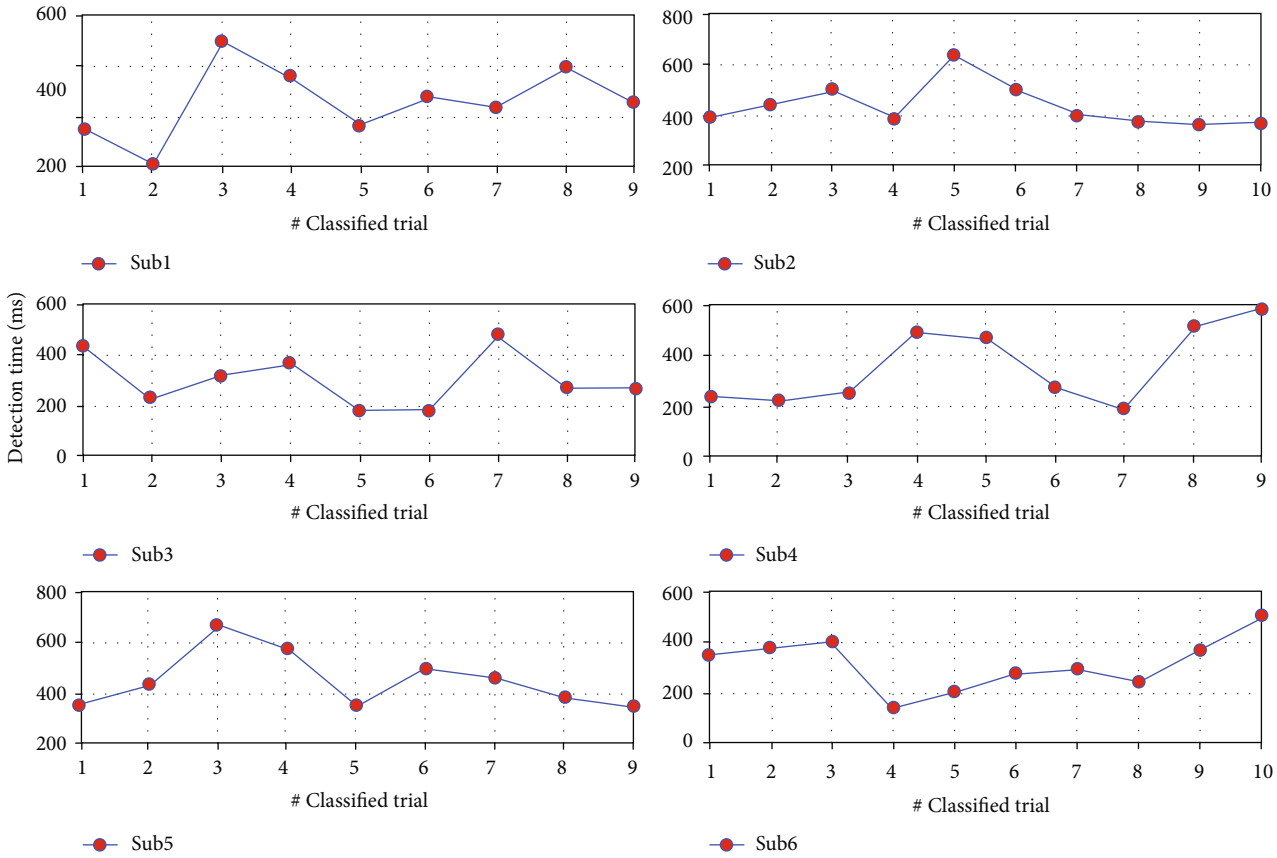

Figure 6: Implemented system detection times assessed on each trial and for each subject involved in the study.

defined six operations from muscle trigger activation to recalibration of thresholds.

The remaining time (~350 ms on average), with its high variability, is strictly related to the selected muscle bundle for the MT function (i.e., lateral gastrocnemius). In fact, it is better to remember that the system starts working from the contraction of the gastrocnemius (right or left independently). The times related to this physiological process remain not determinable with certainty. In this respect, the response times of the gastrocnemius constitute unavoidable delays in recognizing losses of balance and largely determine the efficiency of the system.

To provide a more complete overview of the efficiency, Figure 6 shows the trial-by-trial response times of the implemented system. In the worst case (i.e., Sub 2 and Trial 5), the system takes about 634 ms to intervene, while in the best case (i.e., Sub 6 and Trial 4), the system recognizes the loss of balance in about 160.4 ms.

The achieved detection times are competitive with respect to the state-of-the-art solutions, highlighting the system applicability in contexts of postural recovery strategy implementation.

A final comparative plot with the state-of-the-art solutions is provided in Figure 7. The plot shows the detection time versus the overall accuracy (i.e., mean between Se (%) and Sp (%)), providing an interesting metric for the performance assessment of the PIFD algorithm. Ideally, the algorithms should tend to the bottom-right corner.

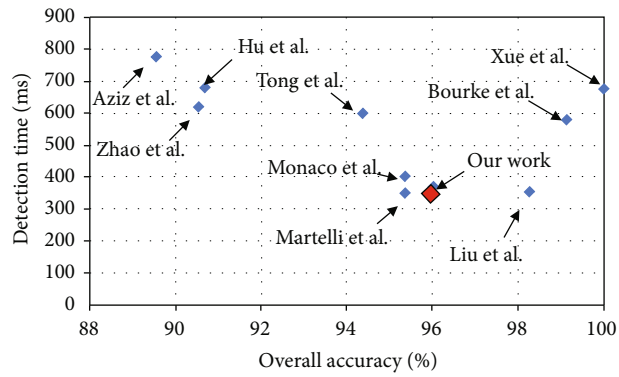

Figure 7: State-of-the-art comparison: detection time (ms) versus accuracy (%).

4. Conclusions

In this paper, a novel methodology that early discriminates an unexpected loss of balance event from ordinary life movements, by analyzing the subjects' cortical signal modifications (at the scalp level) in the time-frequency domain has been presented.

The system was successfully tested and optimized for the early detection of balance losses when unexpected slippages occur during the walking, realizing a first-of-a-kind wearable sensor-based recognition system for induced slippages.

Experimental validation on six young adults demonstrated that the system recognizes a loss of balance with a sensitivity of 93.33% and a specificity of 98.91%. In terms of efficiency, the system asks for 370.62 ms to recognize a balance perturbation.

The here-proposed PIFD strategy has been designed to be low compute intensive and thus suitable for the implementation on a microcontroller or FPGA.

The performance (accuracy and detection time) suggest the technique for real-time applications. Despite this, future perspectives concern the application of the PIFD methodology to a catchment area more relevant to the objective (group of persons 65+), as well as the identification of the proper protection or mitigation strategies (e.g., by using wearable robotic platforms) and the improvement of the acquisition system wearability.

Data Availability

The data used to support the findings of this study are available from the corresponding author upon request.

Conflicts of Interest

The authors declare that there is no conflict of interest regarding the publication of this paper.

Acknowledgments

This work was supported by the project AMICO (Assistenza Medicale In COntextual awareness, AMICO Project ARS01_00900) by the National Programs (PON) of the Italian Ministry of Education, University and Research (MIUR) (Decree no. 267).

References

[1] J. Massion, "Postural control system," *Current Opinion in Neurobiology*, vol. 4, no. 6, pp. 877–887, 1994.

[2] M. P. Murray, A. A. Seireg, and S. B. Sepic, "Normal postural stability and steadiness: quantitative assessment," *The Journal of Bone & Joint Surgery*, vol. 57, no. 4, pp. 510–516, 1975.

[3] D. S. Marigold and J. E. Misiaszek, "Whole-body responses: neural control and implications for rehabilitation and fall prevention," *The Neuroscientist*, vol. 15, no. 1, pp. 36–46, 2009.

[4] J. E. Misiaszek, "Neural control of walking balance: if falling then react else continue," *Exercise and Sport Sciences Reviews*, vol. 34, no. 3, pp. 128–134, 2006.

[5] N. Noury, T. Herve, V. Rialle et al., "Monitoring behavior in home using a smart fall sensor and position sensors," in *1st Annual International IEEE-EMBS Special Topic Conference on Microtechnologies in Medicine and Biology. Proceedings (Cat. No.00EX451)*, pp. 607–610, Lyon, France, 2000.

[6] O. P. Ryynänen, S. L. Kivelä, R. Honkanen, and P. Laippala, "Falls and lying helpless in the elderly," *Zeitschrift für Gerontologie*, vol. 25, no. 4, pp. 278–282, 1992.

[7] S. Chaudhuri, H. Thompson, and G. Demiris, "Fall detection devices and their use with older adults: a systematic review," *Journal of Geriatric Physical Therapy*, vol. 37, no. 4, pp. 178–196, 2014.

[8] X. Hu and X. Qu, "Pre-impact fall detection," *BioMedical Engineering OnLine*, vol. 15, no. 1, p. 61, 2016.

[9] X. Hu and X. Qu, "An individual-specific fall detection model based on the statistical process control chart," *Safety Science*, vol. 64, pp. 13–21, 2014.

[10] D. Martelli, F. Artoni, V. Monaco, A. M. Sabatini, and S. Micera, "Pre-impact fall detection: optimal sensor positioning based on a machine learning paradigm," *PLoS One*, vol. 9, no. 3, article e92037, 2014.

[11] J. Liu and T. E. Lockhart, "Development and evaluation of a prior-to-impact fall event detection algorithm," *IEEE Transactions on Biomedical Engineering*, vol. 61, no. 7, pp. 2135–2140, 2014.

[12] D. A. Winter, *Biomechanics and Motor Control of Human Movement*, John Wiley & Sons, 2009.

[13] A. K. Bourke, K. J. O'Donovan, and G. ÓLaighin, "The identification of vertical velocity profiles using an inertial sensor to investigate pre-impact detection of falls," *Medical Engineering & Physics*, vol. 30, no. 7, pp. 937–946, 2008.

[14] L. Tong, Q. Song, Y. Ge, and M. Liu, "HMM-based human fall detection and prediction method using tri-axial accelerometer," *IEEE Sensors Journal*, vol. 13, no. 5, pp. 1849–1856, 2013.

[15] V. Monaco, P. Tropea, F. Aprigliano et al., "An ecologically-controlled exoskeleton can improve balance recovery after slippage," *Scientific Reports*, vol. 7, no. 1, article 46721, 2017.

[16] N. Pannurat, S. Thiemjarus, and E. Nantajeewarawat, "Automatic fall monitoring: a review," *Sensors*, vol. 14, no. 7, pp. 12900–12936, 2014.

[17] D. De Venuto, V. F. Annese, M. de Tommaso, E. Vecchio, and A. L. Sangiovanni Vincentelli, "Combining EEG and EMG signals in a wireless system for preventing fall in neurodegenerative diseases," in *Ambient Assisted Living*, B. Andò, P. Siciliano, V. Marletta, and A. Monterìù, Eds., vol. 11 of Biosystems & Biorobotics, Springer, Cham, Switzerland, 2015.

[18] V. F. Annese and D. De Venuto, "Fall-risk assessment by combined movement related potentials and co-contraction index monitoring," *2015 IEEE Biomedical Circuits and Systems Conference (BioCAS)*, 2015, pp. 1–4, Atlanta, GA, USA, 2015.

[19] D. de Venuto, D. T. Castro, Y. Ponomarev, and E. Stikvoort, "0.8 μW 12-bit SAR ADC sensors interface for RFID applications," *Microelectronics Journal*, vol. 41, no. 11, pp. 746–751, 2010.

[20] V. F. Annese and D. De Venuto, "The truth machine of involuntary movement: FPGA based cortico-muscular analysis for fall prevention," in *2015 IEEE International Symposium on Signal Processing and Information Technology (ISSPIT)*, pp. 553–558, Abu Dhabi, United Arab, 2015.

[21] D. De Venuto, M. J. Ohletz, and B. Riccò, "Digital window comparator DfT scheme for mixed-signal ICs," *Journal of Electronic Testing*, vol. 18, no. 2, pp. 121–128, 2002.

[22] D. De Venuto and M. J. Ohletz, "On-chip test for mixed-signal ASICs using two-mode comparators with bias-programmable reference voltages," *Journal of Electronic Testing*, vol. 17, no. 3/4, pp. 243–253, 2001.

[23] O. Aziz, C. M. Russell, E. J. Park, S. Member, and S. N. Robinovitch, "The effect of window size and lead time on pre-impact fall detection accuracy using support vector machine analysis of waist mounted inertial sensor data," in *2014 36th Annual International Conference of the IEEE Engineering in Medicine and Biology Society*, pp. 30–33, Chicago, IL, USA, 2014.

[24] Y. Lajoie and S. P. Gallagher, "Predicting falls within the elderly community: comparison of postural sway, reaction time, the Berg balance scale and the Activities-specific Balance Confidence (ABC) scale for comparing fallers and non-fallers," *Archives of Gerontology and Geriatrics*, vol. 38, no. 1, pp. 11–26, 2004.

[25] G. Wu and S. Xue, "Portable preimpact fall detector with inertial sensors," *IEEE Transactions on Neural Systems and Rehabilitation Engineering*, vol. 16, no. 2, pp. 178–183, 2008.

[26] G. Zhao, Z. Mei, D. Liang et al., "Exploration and implementation of a pre-impact fall recognition method based on an inertial body sensor network," *Sensors*, vol. 12, no. 11, pp. 15338–15355, 2012.

[27] D. De Venuto, V. F. Annese, and G. Mezzina, "An embedded system remotely driving mechanical devices by P300 brain activity," in *Design, Automation and Test in Europe Conference and Exhibition (DATE), 2017*, pp. 1014–1019, Lausanne, Switzerland, 2017.

[28] J. P. Varghese, R. E. McIlroy, and M. Barnett-Cowan, "Perturbation-evoked potentials: significance and application in balance control research," *Neuroscience & Biobehavioral Reviews*, vol. 83, pp. 267–280, 2017.

[29] E. Wittenberg, J. Thompson, C. S. Nam, and J. R. Franz, "Neuroimaging of human balance control: a systematic review," *Frontiers in Human Neuroscience*, vol. 11, p. 170, 2017.

[30] A. Mierau, B. Pester, T. Hülsdünker, K. Schiecke, H. K. Strüder, and H. Witte, "Cortical correlates of human balance control," *Brain Topography*, vol. 30, no. 4, pp. 434–446, 2017.

[31] S. Makeig, K. Gramann, T.-P. Jung, T. J. Sejnowski, and H. Poizner, "Linking brain, mind and behavior," *International Journal of Psychophysiology*, vol. 73, no. 2, pp. 95–100, 2009.

[32] J. F. Cavanagh and M. J. Frank, "Frontal theta as a mechanism for cognitive control," *Trends in Cognitive Sciences*, vol. 18, no. 8, pp. 414–421, 2014.

[33] W. Klimesch, R. Fellinger, and R. Freunberger, "Alpha oscillations and early stages of visual encoding," *Frontiers in Psychology*, vol. 2, p. 118, 2011.

[34] A. K. Engel and P. Fries, "Beta-band oscillations — signalling the status quo?," *Current Opinion in Neurobiology*, vol. 20, no. 2, pp. 156–165, 2010.

[35] C. Neuper and G. Pfurtscheller, "Event-related dynamics of cortical rhythms: frequency-specific features and functional correlates," *International Journal of Psychophysiology*, vol. 43, no. 1, pp. 41–58, 2001.

[36] T. Solis-Escalante, J. van der Cruijsen, D. de Kam, J. van Kordelaar, V. Weerdesteyn, and A. C. Schouten, "Cortical dynamics during preparation and execution of reactive balance responses with distinct postural demands," *NeuroImage*, vol. 188, pp. 557–571, 2019.

[37] D. De Venuto and J. Rabaey, "RFID transceiver for wireless powering brain implanted microelectrodes and backscattered neural data collection," *Microelectronics Journal*, vol. 45, no. 12, pp. 1585–1594, 2014.

[38] L. B. Luciani, V. Genovese, V. Monaco, L. Odetti, E. Cattin, and S. Micera, "Design and evaluation of a new mechatronic platform for assessment and prevention of fall risks," *Journal of Neuroengineering and Rehabilitation*, vol. 9, no. 1, p. 51, 2012.

[39] F. Aprigliano, D. Martelli, P. Tropea, G. Pasquini, S. Micera, and V. Monaco, "Aging does not affect the intralimb coordination elicited by slip-like perturbation of different intensities," *Journal of Neurophysiology*, vol. 118, no. 3, pp. 1739–1748, 2017.

[40] D. Martelli, F. Aprigliano, P. Tropea, G. Pasquini, S. Micera, and V. Monaco, "Stability against backward balance loss: age-related modifications following slip-like perturbations of multiple amplitudes," *Gait & Posture*, vol. 53, pp. 207–214, 2017.

[41] M. Sazgar and M. G. Young, "EEG Artifacts," in *Absolute Epilepsy and EEG Rotation Review*, pp. 149–162, Springer, Cham, Switzerland, 2019.

[42] S. Blum, N. S. J. Jacobsen, M. G. Bleichner, and S. Debener, "A Riemannian modification of artifact subspace reconstruction for EEG artifact handling," *Frontiers in Human Neuroscience*, vol. 13, p. 141, 2019.

[43] V. F. Annese and D. De Venuto, "Gait analysis for fall prediction using EMG triggered movement related potentials," in *2015 10th International Conference on Design and Technology of Integrated Systems in Nanoscale Era (DTIS)*, pp. 1–6, Naples, Italy, 2015.

[44] M. Blagojevic, M. Kayal, M. Gervais, and D. De Venuto, "SOI hall-sensor front end for energy measurement," *IEEE Sensors Journal*, vol. 6, no. 4, pp. 1016–1021, 2006.

[45] S. Carrara, M. D. Torre, A. Cavallini, D. De Venuto, and G. De Micheli, "Multiplexing pH and temperature in a molecular biosensor," in *2010 Biomedical Circuits and Systems Conference (BioCAS)*, pp. 146–149, Paphos, Cyprus, 2010.